*J. Fluid Mech.* (1993), *vol.* 255, *pp.* 157–182



# Tearing of an aligned vortex by a current difference in two-layer quasi-geostrophic flow

By J. S. MARSHALL AND B. PARTHASARATHY
Department of Ocean Engineering, Florida Atlantic University, Boca Raton, FL 33431, USA

(Received 16 October 1992 and in revised form 29 March 1993)

A study of two-layer quasi-geostrophic vortex flow is performed to determine the effect of a current difference between the layers on a vortex initially extending through both layers. In particular, the conditions under which the vortex can resist being torn by the current difference are examined. The vortex evolution is determined using versions of the contour dynamics and discrete vortex methods which are modified for two-layer quasi-geostrophic flows. The vortex response is found to depend upon the way in which the current difference between the layers is maintained. In the first set of flows studied, the current difference is generated by a (stronger) third vortex in the upper layer located at a large distance from the (weaker) vortex under study. Flows of this type are important for understanding the interactions of vortices of different sizes in geophysical turbulence. A set of flows is also considered in which an ambient geostrophic current difference is produced by a non-uniform background potential vorticity field. In this case, an additional (secondary) flow field about the vortex patch in each layer is generated by redistribution of the ambient potential vorticity field.

It is found that a vortex that initially extends through both layers will undergo a periodic motion, in which the two parts of the initial vortex in the different layers (called the 'upper' and 'lower' vortices) oscillate about each other, provided that the current difference between the layers is less than a critical value. When the current difference exceeds this critical value, the upper and lower vortices separate permanently and the initial vortex is said to 'tear'. The effects of various dimensionless parameters that characterize the flow are considered, including the ratio of core radius to internal Rossby radius, the ratio of layer depths and the ratio of the strengths of the upper and lower vortices. These parameters affect both the critical current difference for tearing and the deformation of the vortex cores by their interaction. It is found that for small values of inverse internal Rossby deformation radius, calculations with circular non-deformable vortices (convected at their centrepoints) give results in good agreement with the contour dynamics simulations, since the vortex deformation is small. The results of the study will be useful in determining the conditions under which large geophysical vortex structures, such as cyclones and ocean rings, can extend to large heights (depths) even though the mean winds (currents) in the ambient flow change significantly along the vortex length.

## 1. Introduction

The atmosphere and oceans are often modelled, for purposes of geophysical flow calculation, by a set of nearly homogeneous layers separated by regions of strong density stratification, where the stratified regions are usually taken to be of infinitesimal thickness. Large-scale oceanic flows, for instance, can be crudely modelled using a two-layer system consisting of a shallow surface layer and a much deeper 'deep-water' layer

separated by the 'thermocline'. Vortices in geophysical systems (with constant Coriolis parameter) consist of a region of potential vorticity surrounded by fluid with a different potential vorticity (not necessarily uniform), where we recall that potential vorticity is an invariant of motion for inviscid flows with small Rossby number. A vortex whose potential vorticity exists in one layer can cause motion of the fluid in adjoining layers by displacement of the interface separating the layers. Two vortices in different layers can thus induce motion of each other and interact in much the same way as a vortex pair in usual two-dimensional hydrodynamics. The 'heton' described by Hogg & Stommel (1985), which consists of a translating pair of vortices with opposite potential vorticity in two different layers, provides a well-known example of baroclinic vortex interaction.

The general equations for two-layer quasi-geostrophic flow can be found in the text by Pedlosky (1979, pp. 386–394). A study of interaction of systems of singular quasi-geostrophic vortices in two-layer systems is given by Gryanik (1983), including a Hamiltonian formulation. The stability of quasi-geostrophic vortices with finite core radius is studied by Helfrich & Send (1988) and Flierl (1988), both analytically and numerically, using a contour dynamics method adopted for two-layer geostrophic flows. It is found that a necessary condition for instability of a system consisting of an upper-layer vortex positioned directly above a lower-layer vortex, in which both vortices are initially circular and have the same core radii, is that the potential vorticity of the vortices (minus that in the ambient flow) must be of opposite sign. Merger of vortices in two layers is studied by Polvani, Zabusky & Flierl (1989) and Polvani (1991), again using the contour dynamics approach. Of particular interest in this work is the finding that two vortices in different layers, in which the vortex centres are initially separated by some distance $d_c$, may 'align' over each other in a process that appears very similar to merger of two vortices in ordinary two-dimensional hydrodynamics. Results for vortices with equal potential vorticity show that alignment occurs only for a range of intermediate separation distances in which the vortex centres are neither too close together nor too far apart and for a range of dimensionless internal Rossby radii less than some critical value. Some experiments demonstrating heton formation and vortex merger in two-layer rotating systems were performed by Griffiths & Hopfinger (1986, 1987).

Reznik (1992) and Gryanik (1986) extended the singular vortex analysis for single-layer quasi-geostrophic flows to include the beta-effect. In this case, the ambient flow field has a non-uniform potential vorticity due to the beta-effect, and the redistribution of this ambient potential vorticity by the singular vortices generates a secondary flow about the vortices (which Reznik calls the 'regular' flow). Although it does not seem to have been studied previously in any depth, a mean unidirectional current difference between the layers of a two-layer quasi-geostrophic flow in an $f$-plane can be generated by a non-uniform ambient potential vorticity field, and vortex motion superimposed on such a current would also produce a secondary flow about the vortices.

Geophysical vortex formation and motion is a major contributor to fluid mixing and heat transfer both between different vertical layers in the oceans and atmosphere and between adjacent water or air masses. Horizontal mixing of water masses due to oceanic 'rings', formed by dynamic instabilities of currents, and tropical cyclones in the atmosphere play an important role in modifying the climate of local regions and in providing a net transfer of heat toward the poles. Vertical mixing by atmospheric cyclones causes cloud formation, which both provides fresh water transfer and increases the atmospheric absorption and backscatter of long-wave radiant energy. Vertical mixing (or 'deep water production') in the oceans is important in determining

the rate of average temperature change of the Planet due to variation of the net radiant energy balance, since the oceanic deep water is the major planetary thermal energy storage reservoir. Deep water production in the open ocean has frequently been associated with intense eddies passing through the entire water column, which may form convective 'chimneys' that are thought to be responsible for open-ocean polynyas (Gordon 1978; Killworth 1979) or may form as topographically trapped eddies within a Taylor column (Hogg 1973; Eide 1979).

In both the oceans and the atmosphere, the intense eddies responsible for vertical mixing usually extend entirely through two or more stratified layers, even though the mean currents may be very different in the layers. On the other hand, less intense eddies, which may cause horizontal but not usually vertical mixing between layers, often exist in only one layer, and are therefore not subject to a large current variation along their lengths. This observation is the motivation for the present research. In particular, we seek to determine the conditions such that a vortex which initially extends through two layers (or in which the upper and lower layer vortices are initially aligned) will remain aligned (or nearly so) when a mean current difference is applied between the layers.

The vortex response to the current difference is found to depend somewhat on the manner in which the current difference is generated. In the present paper, we first consider cases in which the current difference between the layers is generated by a third, and much stronger, vortex located in the upper layer at a large distance from the vortex under consideration. This problem is important for understanding interaction of vortices of different strengths in geophysical turbulence. The tearing of the vortex is first studied using three circular vortices, convected at their central points, which demonstrates the main phenomenon under consideration. Calculations are then performed using the contour dynamics and vortex 'cloud' methods to determine the effect of vortex deformation on these results. It is found that when the current difference between the layers is less than some critical value (which varies with vortex strength and core radius and with ambient oceanic conditions), the vortices in the two layers will undergo a periodic oscillation in which the maximum distance separating the vortex centres is proportional to the mean current difference. For sufficiently small current differences (or for sufficiently intense vortices), the amplitude of the periodic motion is so small that the vortex will appear to simply extend through the layers with little effect of the mean currents. If the current difference is above this critical value, however, the vortices in the two layers separate permanently, in which case we say that the current 'tears' the vortex.

Next, calculations are performed to study vortex tearing for the case in which the current difference is maintained by a non-uniform background potential vorticity distribution. This problem is important for determining the effect of mean geostrophic currents (winds) on large-scale vortices in the oceans and atmosphere. The redistribution of the background potential vorticity field causes a secondary flow to form about the vortices, but the response of the vortices to the current difference is similar to that in the three-vortex problem.

The general equations governing quasi-geostrophic vortex flow and their solutions in terms of Green's functions are recalled in §2 of the paper. Two different approaches to numerical solution of these equations are described in §3, using a contour dynamics approach and a discrete vortex algorithm adapted to two-layer quasi-geostrophic flows. A finite-difference algorithm for solution of the secondary flow field due to redistribution of a non-uniform ambient potential vorticity is also described in §3. Numerical and analytical results for cases with three circular vortices, which

demonstrate the main phenomenon under consideration, are presented in §4. In §5, the effect of core deformation on these results is studied using contour dynamics and vortex 'cloud' simulations, again for the three-vortex interaction problem. In §6, the effect of secondary flow caused by a non-uniform background potential vorticity field is studied. Conclusions of the study are given in §7.

## 2. Basic theory

The governing equations for quasi-geostrophic two-layer flow in an $f$-plane for cases in which the density difference $\Delta\rho$ is small compared to the density $\rho$ in either layer are given by Pedlosky (1979) as

$$\nabla^2\psi_n + (-1)^n F_n(\psi_1 - \psi_2) = q_n. \tag{1}$$

In (1), $\psi_n$ is the stream function in layer $n$, where $n = 1$ for the upper layer and $n = 2$ for the lower layer, defined by $u_n = -\partial\psi_n/\partial y$ and $v_n = \partial\psi_n/\partial x$, and $q_n$ is the potential vorticity at some point $\boldsymbol{x}$ (multiplied by the equilibrium layer depth and minus the Coriolis parameter). For a quasi-geostrophic flow, $q_n$ is independent of time at any given material point. The internal Froude numbers $F_n$ for the two layers are defined by

$$F_n = f_c^2 R^2/g' H_n, \tag{2}$$

where $f_c$ is the (constant) Coriolis parameter, $R$ is the initial eddy radius (which is taken to be the same for all eddies), $H_n$ is the ambient depth of layer $n$ and $g'$ is the reduced gravity $g\Delta\rho/\rho$. It is clear that $F_n$ is simply the square of the eddy core radius divided by the internal Rossby radius of the layer. We non-dimensionalize all length variables by $R$ and all time variables by a timescale $T$, which will be specified later in the paper. Velocities are non-dimensionalized by $R/T$, and stream functions by $R^2/T$, and so on. A schematic diagram of the initial configuration for the two-layer vortex pair given in figure 1 illustrates the various flow parameters.

The two layers communicate with each other by a displacement $\eta_I$ of the interface separating the layers. The bottom surface of the lower layer is taken as horizontal and fixed, but the top surface of the upper layer may be displaced by an amount $\eta_T$. The surface displacements are related to the stream functions $\psi_n$ by

$$\eta_I = f_c(\psi_2 - \psi_1)/g', \quad \eta_T = f_c\psi_1/g. \tag{3}$$

We note that $\eta_I$ will be much greater than $\eta_T$ whenever $\Delta\rho \ll \rho$, such that $g' \ll g$, which is assumed throughout the paper.

An alternative form of these equations can be written in terms of the barotropic and baroclinic stream functions $\psi_B$ and $\psi_T$, respectively, and potential vorticities $q_B$ and $q_T$, defined by

$$\psi_B = \psi_1 + \psi_2/\delta, \quad \psi_T = \psi_1 - \psi_2, \tag{4a}$$

$$q_B = q_1 + q_2/\delta, \quad q_T = q_1 - q_2, \tag{4b}$$

where $\delta = H_1/H_2$ is the height ratio. Using (4), (1) gives independent equations for $\psi_B$ and $\psi_T$ as

$$\nabla^2\psi_B = q_B, \quad \nabla^2\psi_T - k^2\psi_T = q_T, \tag{5a, b}$$

where $k^2 = F_1 + F_2$.

In solving (5), we first consider cases where $q_n$ vanishes outside compact (vortical) regions, which will be used in §§4 and 5 of the paper. For later convenience, we attach a subscript $v$ to variables such as $\psi$, $q$ and the horizontal velocity components $u$ and $v$ to denote the contributions from the vortices in the flow. Equation (5) can be solved

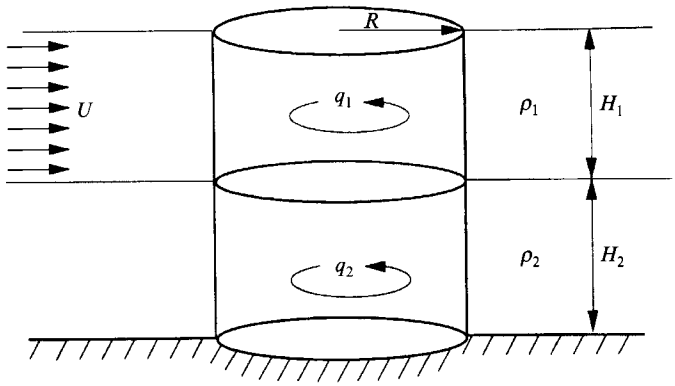


FIGURE 1. Schematic showing the initial configuration of the aligned vortex pair with two-layer density stratification and current flow in the upper layer.

using the Green's functions $\ln(r)/2\pi$ for the barotropic component in (5*a*) and $-K_0(kr)/2\pi$ for the baroclinic component in (5*b*), where $K_0(\cdot)$ is the modified Bessel function of the second kind, giving solutions of the form

$$\psi_{Bv}(x,y,t) = \frac{1}{2\pi}\int_{-\infty}^{\infty}\int_{-\infty}^{\infty} q_{Bv}(\xi,\eta,t)\ln(r)\,\mathrm{d}\xi\,\mathrm{d}\eta, \tag{6a}$$

$$\psi_{Tv}(x,y,t) = -\frac{1}{2\pi}\int_{-\infty}^{\infty}\int_{-\infty}^{\infty} q_{Tv}(\xi,\eta,t)\,K_0(kr)\,\mathrm{d}\xi\,\mathrm{d}\eta, \tag{6b}$$

where $r^2 = [(x-\xi)^2+(y-\eta)^2]$. Substituting expressions for $q_{Tv}$ and $q_{Bv}$ into (6) and taking $(-\partial/\partial y, \partial/\partial x)$, after using (4), gives the velocity field $(u_n, v_n)$ in the two layers.

The simplest potential vorticity distribution that admits core deformation is that in which the potential vorticity is uniform within one or more regions $C_n$ and is equal to another constant (which can be taken as zero without loss in generality) outside of $C_n$. In this case, Green's theorem can be used to convert the integrals in (6*a*, *b*) over $q_{Bv}$ and $q_{Tv}$ to integrals over the contour $C_n$. The resulting solution for the components $u_{vn}$ and $v_{vn}$ of the velocity field (in layer $n$) generated by the vortices is given by

$$u_{vn}(x,y,t) = \frac{\delta}{2\pi(1+\delta)}\sum_{m=1}^{2}\int_{C_m}[a_{n,m}\ln(r)+b_{n,m}K_0(kr)]\,\mathrm{d}\xi, \tag{7a}$$

$$v_{vn}(x,y,t) = \frac{\delta}{2\pi(1+\delta)}\sum_{m=1}^{2}\int_{C_m}[a_{n,m}\ln(r)+b_{n,m}K_0(kr)]\,\mathrm{d}\eta, \tag{7b}$$

where $\mathrm{d}\xi$ and $\mathrm{d}\eta$ are the components of an infinitesimal vector $\mathrm{d}\boldsymbol{x}$ along $C_m$ in the $x$- and $y$-directions, respectively, and the integration is performed in a counterclockwise direction. The components $a_{n,m}$ and $b_{n,m}$ are defined by

$$\begin{bmatrix} a_{1,1} & a_{1,2} \\ a_{2,1} & a_{2,2} \end{bmatrix} = \begin{bmatrix} -q_{v1} & -q_{v2}/\delta \\ -q_{v1} & -q_{v2}/\delta \end{bmatrix},$$

$$\begin{bmatrix} b_{1,1} & b_{1,2} \\ b_{2,1} & b_{2,2} \end{bmatrix} = \begin{bmatrix} q_{v1}/\delta & -q_{v2}/\delta \\ -q_{v1} & q_{v2} \end{bmatrix}.$$

For cases in which a non-uniform background potential vorticity field exists, a secondary flow about the vortices is generated by redistribution of the background potential vorticity by the vortex motion. In the case under consideration in §6 of the

paper, the potential vorticities $q_n$ are chosen initially as the sum of that for a vortex of unit radius centred at the origin with uniform potential vorticity within its core and that for a uniform current difference $\Delta U$ in the $x$-direction between the layers. The initial potential vorticity field is thus given by

$$q_n(0) = q_{vn}(0) + q_{cn}(0), \quad q_{cn}(0) = -(-1)^n F_n(\Delta U)\, y, \tag{8}$$

where $q_{vn}(0)$ vanishes for $r > 1$ and is constant for $r \leqslant 1$.

We note that $q_n$ is constant at a material point (or $\mathrm{d}q_n/\mathrm{d}t = 0$). At any later time $t$, the potential vorticity field $q_n$ is decomposed as the sum of the part $q_{vn}$ due to the vortices, the part $q_{cn}$ required to produce a uniform current in the upper layer, and the part $q_{sn}$ due to redistribution of the non-uniform ambient potential vorticity field by the vortices. The part $q_{vn}$, which is taken to be invariant at a material point, will be uniform inside some material region bounded by the closed curve $C_n(t)$ and zero outside this region, where $C_n$ initially coincides with the unit circle. To produce a uniform current in the surface layer, the part $q_{cn}$ must equal its initial value $q_{cn}(0)$ for all later times, so it will in general vary with time at a material point as the fluid particles are deflected by the vortex flow fields. The part $q_{sn}$ is determined from the condition that $\mathrm{d}q_n/\mathrm{d}t$ vanish everywhere in the flow, such that the sum $q_{cn} + q_{sn}$ is invariant at each material point. Initially $q_{sn}$ vanishes, but as the vortices distort the uniform current a non-zero $q_{sn}$ field will form to create a secondary flow about the vortices. From the requirement that the total potential vorticity $q_n$ is invariant at each material point, and since $q_{vn}$ is also invariant, the material derivative of $q_{cn} + q_{sn}$ must vanish everywhere. Using (8) for $q_{cn}$, an equation to determine $q_{sn}$ is obtained as

$$\frac{\partial q_{sn}}{\partial t} + (\boldsymbol{u}_n \cdot \boldsymbol{\nabla})\, q_{sn} = (-1)^n F_n(\Delta U)\, v_n, \tag{9}$$

where $u_n$ and $v_n$ are the components of the total velocity field $\boldsymbol{u}_n$.

The stream function $\psi_n$ in each layer can also be decomposed as the sum of a part $\psi_{vn}$ related to the vortex-induced flow, a part $\psi_{cn}$ due to the uniform current in the upper layer and a part $\psi_{sn}$ due to the secondary flow about the vortices. Each of these parts $\psi_{vn}$, $\psi_{cn}$ and $\psi_{sn}$ satisfies (1) with $q_n$ replaced by the respective part $q_{vn}$, $q_{cn}$ or $q_{sn}$. A solution for $\psi_{cn}$ yielding a uniform current in the upper layer can immediately be obtained as

$$\psi_{c1} = C - (\Delta U)\, y, \quad \psi_{c2} = C, \tag{10}$$

where $C$ is an arbitrary constant. Barotropic and baroclinic potential vorticities and stream functions can be defined for both the vortex-induced flow and the secondary flow as in (4$a$, $b$) to yield decoupled equations similar to those in (5). Solutions for $\psi_{vn}$ are the same as displayed in (6$a$) and (6$b$). Since $q_{vn}$ are still chosen to be uniform within a closed contour $C_n$, we can still use Green's theorem to transform the surface integral in (6) into a contour integral for $u_{vn}$ and $v_{vn}$, as shown in (7). The secondary vorticity $\psi_{sn}$ satisfies the Poisson and Helmholtz equations

$$\nabla^2 \psi_{Bs} = q_{Bs}, \quad \nabla^2 \psi_{Ts} - k^2 \psi_{Ts} = q_{Ts}, \tag{11}$$

where the barotropic and baroclinic components $q_{Bs}$ and $q_{Ts}$ of $q_{sn}$ are defined similarly to $q_B$ and $q_T$ in (4). If we assume that $q_{sn}$ decays sufficiently fast at infinity, the Green's functions can again be used to write the solution to (11) in terms of integrals, with a form similar to (6), over the entire flow field. The reduction to a contour integral cannot be performed, since $q_{sn}$ varies continuously over the flow field. It is often more computationally efficient for very large grids, however, to solve (11) directly using a fast (spectral) solver for the Helmholtz equation.

## 3. Numerical approaches

### 3.1. *Contour dynamics approach to determine* $\psi_{vn}$

To determine the velocities induced by the vortices, the integrals in (7*a*, *b*) are evaluated using Simpson's rule with 50 intervals about each contour $C_n$. The local singularity as $(\xi, \eta) \to (x, y)$ for each position on the contour is integrable and is evaluated explicitly. The points on the contours are convected as material points in the flow, so that the motion of each point $(x_n(t), y_n(t))$ on $C_n(t)$ is given by

$$\frac{\mathrm{d}x_n}{\mathrm{d}t} = u_n(x_n, y_n, t), \quad \frac{\mathrm{d}y_n}{\mathrm{d}t} = v_n(x_n, y_n, t), \tag{12}$$

where $u_n$ and $v_n$ are the components of the total velocity vector. The solution for $x_n$ and $y_n$ is advanced in time using a two-step predictor–corrector method. The timescale $T$ is set equal to $T = (1+\delta)/(\delta q_{v1} + q_{v2})$, and the reason for this choice is explained in §4. The dimensionless timestep $\Delta t$ was fixed at 0.1 for all runs. Variation of the timestep within a factor of 5 of the value used produces no detectable change in the results.

The contours $C_n$ tend to become jagged and then to break up after some time during the computation. We attribute this instability to filamentation of the vortex, as observed by Polvani (1991) and Pullin (1992), which occurs at scales smaller than that used to discretize the contours. While filamentation is a physical effect, rather than an artifact of the numerical method, it does not usually occur until late in the runs and does not seem to be important for the tearing phenomenon under consideration in the paper. To delay instability of the vortex contour, the changes in the contours are smoothed at every timestep using a spectral filter suggested by Orszag & Gottlieb (1980). In this filter, the contour is represented by a Fourier series which is truncated after 10 modes, and then the Fourier coefficients of the higher-order modes are made to decrease gradually to zero before the contour positions are reformulated. Use of the filter is partially justified by the close comparison between the contour dynamics and discrete vortex simulations.

The computations were tested by comparing with Polvani's (1991) simulations of vortex alignment in two layers and by comparison with the analytical solution for a two-layer geostrophic circular vortex given by Helfrich & Send (1988). The area of the vortices was also computed during the calculations and found to change by less than 5% prior to onset of the instability described in the previous paragraph.

### 3.2. *Discrete vortex approach to determine* $\psi_{vn}$

A two-layer geostrophic version of the discrete vortex method is used as an alternative numerical approach which does not require filtering and which will admit filamentation and breakup of the vortex patches in the two layers. In this approach, we represent each vortex patch as a cloud of singular vortices, such that $q_{vn}$ becomes

$$q_{vn}(\boldsymbol{x}, t) = \sum_{i=1}^{M_n} s_n^i \, \delta[\boldsymbol{x} - \boldsymbol{x}_n^i(t)], \tag{13}$$

where $s_n$ is the strength and $x_n(t)$ the position of the $i$th vortex in layer $n$. The strengths of all point vortices are constant in time and are prescribed to be uniform in a given layer, denoted by $s_n$. The point vortex strength $s_n$ is set such that if $N$ point vortices are used to represent the initially circular vortex patch with potential vorticity $q_{vn}$ in layer $n$, then $s_n = q_{vn}/2N$.

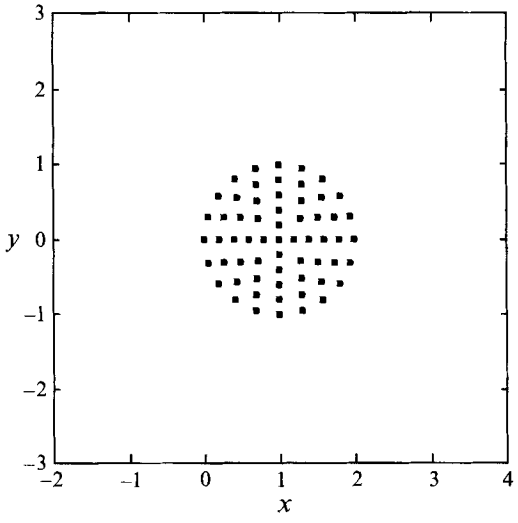


FIGURE 2. Close-up view (from above) showing the initial placement of singular vortices in a vortex patch.

Each singular vortex of strength $s_n$ in layer $n$ induces a circulatory velocity field about it centre. The velocity magnitude $V_{nm}(r)$ in layer $n$ at a distance $r$ from the centre of a point vortex located in layer $m$ is given by

$$V_{nm}(r) = \frac{s_m}{1+\delta}[\delta^{2-m}/r + (-1)^{m-1}(-\delta)^{n-1}kK_1(kr)]. \tag{14}$$

For $\delta = 1$, (14) reduces to the well-known form given by Hogg & Stommel (1985).

The point vortices are convected as material points in the flow, and their motion is advanced with time using a two-step predictor–corrector algorithm. Clouds of 61 point vortices are used in the calculations for both upper- and lower-layer vortex patches. The point vortices are distributed evenly across the vortex patch in the initial configuration, as shown in figure 2, in order to achieve a uniform potential vorticity distribution. The timestep is $\Delta t = 0.1$, which is the same as used in the contour dynamics computations. The predictions of the discrete vortex method were checked by comparison with results for heton pairs by Hogg & Stommel (1985) and with the results from the contour dynamics simulations. The Hamiltonian for two-layer quasi-geostrophic systems of point vortices (Gryanik 1983) was found to be conserved in these calculations to better than one part in 1000.

### 3.3. *Finite-difference approach to determine* $\psi_{sn}$

For the flows considered in §6, a secondary flow arises from redistribution of the non-uniform background potential vorticity field. To determine $q_{sn}$ at each timestep, (9) was solved on a grid that covered the region about the vortex patches in each layer. A centred three-point finite-difference approximation was used for the spatial derivatives and a second-order predictor–corrector scheme was used in time (in conjunction with the solution for $\psi_{vn}$). For a given $q_{sn}$-field at any time, the stream function $\psi_{sn}$ of the secondary flow was obtained from solution of (10) using the fast (spectral) solver for the Helmholtz equation available through IMSL. A square grid with 65 increments on each side was used to span an area covering the vortices measuring 20 vortex core radii on each side.

The fast solver for the Helmholtz equations was found to produce rather noisy results. To reduce this noise, a low-pass spectral filter was applied to the $q_{sn}$-field at each timestep. Alternatively, for some calculations, the $\psi_{sn}$-field was solved using the Green's function solution (6), with subscript $v$ replaced by subscript $s$, where the integrals were performed using the trapezoidal rule. When using this method, a coarser grid with 33 increments on each side was used; however, the results were much less noisy than those obtained by the spectral method. After appropriate filtering of the spectral results, the calculations obtained by the two methods were found to be very similar.

## 4. Results for three circular vortices

In §§4 and 5, we will consider a simple flow (shown in figure 3) in which two circular vortices, with unit core radius, are initially placed on top of each other (one in the upper layer and one in the lower layer), and a current difference between these vortices is generated by a third vortex located in the upper layer at a distance $d$ from the first two vortices. It is assumed that $d \gg 1$ and that the strength of the third vortex is large compared to that of the other two. In order to reduce the problem to its essential features, it is assumed in the present section that all vortices remain circular for all time and are convected at their central points. A solution of (5) for a circular (Rankine) vortex is given by Helfrich & Send (1988) with azimuthal velocity magnitude

$$\bar{V}_n(r) = \frac{1}{1+\delta}\begin{cases}\delta q_B\, r/2 + (-\delta)^{n-1} q_T K_1(k) I_1(kr) & (r \leqslant 1)\\ \delta q_B/2r + (-\delta)^{n-1} q_T I_1(k) K_1(kr) & (r > 1).\end{cases} \tag{15}$$

Using the expressions for $q_B$ and $q_T$ in (4*b*), the velocity magnitude due to a circular vortex with uniform potential vorticity $q_i$ centred at $(x_i, y_i)$ in layer $m$ and evaluated at a point $(x, y)$ in layer $n$ can be obtained from (15) as

$$\bar{V}_{nm}(r_i) = \frac{1}{1+\delta}\begin{cases}(\delta^{2-m})\, r_i\, q_i/2 + (-1)^{m-1}(-\delta)^{n-1} q_i K_1(k) I_1(kr_i) & (r \leqslant 1)\\ (\delta^{2-m})\, q_i/2r_i + (-1)^{m-1}(-\delta)^{n-1} q_i I_1(k) K_1(kr_i) & (r > 1),\end{cases} \tag{16}$$

where $r_i = [(x_i - x)^2 + (y_i - y)^2]^{\frac{1}{2}}$. Comparing (16) with the expression (14) for point vortices, we note that the baroclinic terms in the two expressions are not the same even for $r > 1$. For small values of $k$ (i.e. for cases where the core radius is small compared to the internal Rossby deformation length), $I_1(k) \sim \frac{1}{2}k$ and (16) and (14) become identical (after writing $s = \frac{1}{2}q$ as indicated just prior to (14)).

The equations of motion for a three-vortex system are given by

$$\frac{\mathrm{d}x_i}{\mathrm{d}t} = -\sum_{\substack{j=1\\ j\neq i}}^{3} \frac{y_i - y_j}{r_{ij}} \bar{V}_{n_i n_j}(r_{ij}), \quad \frac{\mathrm{d}y_i}{\mathrm{d}t} = \sum_{\substack{j=1\\ j\neq i}}^{3} \frac{x_i - x_j}{r_{ij}} \bar{V}_{n_i n_j}(r_{ij}), \tag{17}$$

where $r_{ij}$ is the horizontal separation distance between vortex $i$ and vortex $j$ and $n_i$ is the layer number of vortex $i$. We are particularly interested in cases for which $d \gg 1$, such that the third vortex imposes a nearly uniform current difference on the other two vortices of magnitude

$$\Delta U = q_3 I_1(k) K_1(kd). \tag{18}$$

This limit is really only practicable for small values of $k$, since $K_1(kd)$ decays as $(\pi/2kd)^{\frac{1}{2}} \mathrm{e}^{-kd}$ for $kd \gg 1$.

Equation (17) was solved using a fourth-order Runga–Kutta integration in time to obtain plots of the paths of the vortex centres for the initial configuration shown in

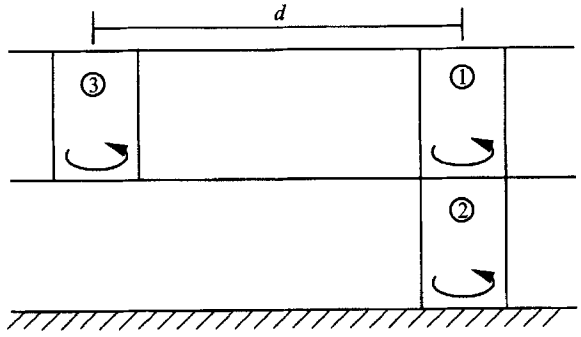


FIGURE 3. Initial configuration for the three-vortex system.

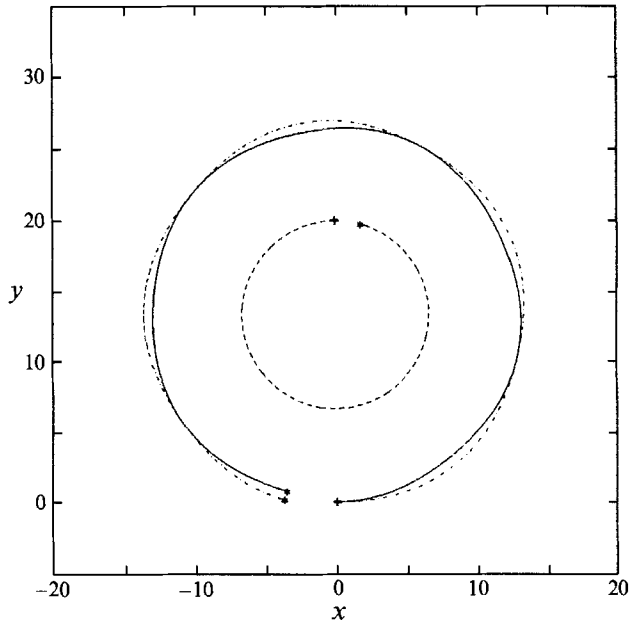


FIGURE 4. Plot of vortex paths for a non-tearing case with $k = 0.2$, $q_1/q_2 = 1$, $\delta = 1$, $\Delta U = 0.005$ and $d = 20$. The initial locations of the vortices (at $t = 0$) are marked + and the final locations (at $t = 1600$) are marked with a *. The paths of vortices numbered 1, 2 and 3 in figure 3 are denoted by solid, dash-dotted and dashed curves, respectively. This convention is also followed in figures 5, 8, 10 and 11.

figure 3. The resulting vortex behaviour can be classified into two types, separated by a clear bifurcation, depending on the value of the current difference $\Delta U$ imposed on the two initially aligned vortices by the third vortex. In the first type of behaviour, the two initially aligned vortices oscillate about each other periodically. This periodic behaviour occurs when the current different $\Delta U$ is below some critical value $\Delta U_{crit}$, which varies with parameters such as $k$, $\delta$, $d$ and the strengths of the vortices. When $\Delta U$ is much below the critical value, the maximum separation distance between the vortex centroids can be much less than the core radius. This type of behaviour is referred to as the non-tearing regime and is demonstrated in figure 4 for the parameter values $(\delta, k, q_1/q_2, \Delta U, d) = (1, 0.2, 1, 0.005, 20)$. The '+' symbols denote the initial locations of the vortices (at $t = 0$) and the '*' symbols denote the final locations at the end of the calculation ($t = 1600$). The two initially aligned vortices are observed to separate slightly (by a

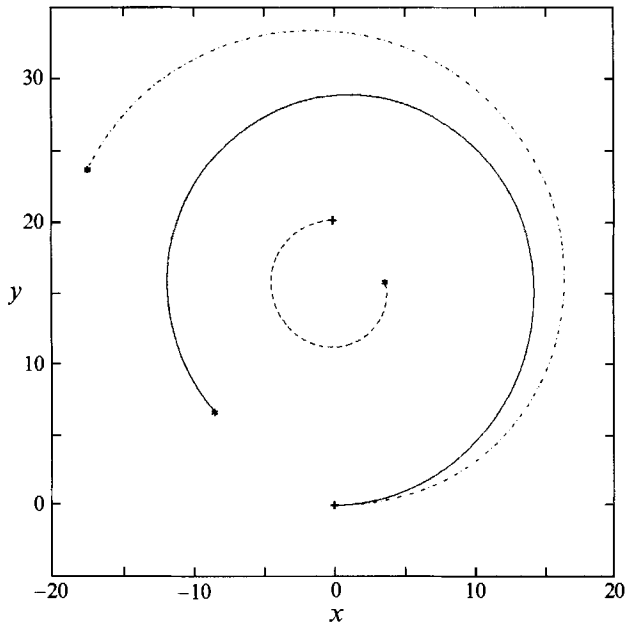


FIGURE 5. Plot of vortex paths for a tearing case with $\Delta U = 0.0088$ and all other parameters and symbols the same as in figure 4. The final locations are at $t = 800$.

distance much less than $d$) and then rejoin four times during the calculation. Both the third vortex and the two initially aligned vortices are observed to rotate in circles, but the distance $d$ between the third vortex and the mean location of the first two vortices is nearly constant during the motion.

As $\Delta U$ is raised above the critical value $\Delta U_{crit}$, the vortex motion changes dramatically to a regime in which the two initially aligned vortices no longer oscillate about each other, but are instead torn apart by the current difference imposed by the third vortex. This type of behaviour is illustrated in figure 5 for the same parameter values as in figure 4, but with a higher current difference ($\Delta U = 0.0088$). The final positions are at $t = 800$. The two initially aligned vortices separate such that the upper-layer vortex, which experiences a greater current from the third vortex, rotates faster about the third vortex than the lower-layer vortex. In this type of behaviour, the current difference imposed between the two initially aligned vortices is so strong that their mutually induced velocity is not sufficient to maintain the periodic oscillation about each other observed in figure 4. For short times, such as shown in figure 5, it appears that the current difference has caused a permanent separation of the initially aligned vortices in the vortex tearing case. However, we note that any motion of a three-vortex system in a two-layer quasi-geostrophic flow can in general be shown to be periodic. (The proof, which uses an argument similar to that of Aref & Pomphrey 1982, is based on the fact that any $N$-vortex problem in a two-layer quasi-geostrophic flow is a Hamiltonian system with three integrals in involution, from which it follows that the three-vortex system must be integrable.) If the computations are allowed to proceed for a very long time, we indeed find that the upper-layer vortex 'laps' the lower-layer vortex and for an instant the two become aligned again. This type of oscillation, which occurs on a very long timescale and exhibits large separation of the vortices, can be clearly distinguished from the short-period oscillation with small separation of the initially aligned vortices in the non-tearing case observed in figure 4.

Further insight into the nature of the periodic oscillation of the vortices in the non-tearing regime can be obtained by assuming that $d$ is much larger than the separation distance between the two initially aligned vortices for all time, for which case the two initially aligned vortices and the third vortex behave approximately as a two-body system and the separation distance $d$ and the rotation rate $\Omega$ of the system are constants. Based on this assumption, a system of equations can be obtained from (16) and (17) for the relative displacements $\xi = x_1 - x_2$ and $\eta = y_1 - y_2$ of the first two vortices (which are initially zero) as

$$\frac{\mathrm{d}\xi}{\mathrm{d}t} = -\eta f(r) - \Delta U \sin(\Omega t), \quad \frac{\mathrm{d}\eta}{\mathrm{d}t} = \xi f(r) + \Delta U \cos(\Omega t), \tag{19}$$

where, with timescale $T = (1+\delta)/(\delta q_1 + q_2)$, $f(r)$ depends only on $k$ and the separation distance $r = (\xi^2 + \eta^2)^{\frac{1}{2}}$ between the first two vortices and is defined by

$$f(r) = \begin{cases} 1/2r^2 - (1/r) I_1(k) K_1(kr) & (r > 1) \\ 1/2 - (1/r) K_1(k) I_1(kr) & (r \leqslant 1). \end{cases} \tag{20}$$

A linear solution of system (19) can be obtained by noting that for small values of the separation distance $r$ between the vortex centres, (20) becomes

$$f(r) \sim \tfrac{1}{2}[1 - kK_1(k)] \equiv \omega(k), \tag{21}$$

which is independent of $r$. We denote the limit in (21) by the parameter $\omega(k)$. In this small-displacement limit, (19) reduces to the linear system

$$\frac{\mathrm{d}\xi}{\mathrm{d}t} = -\omega\eta - \Delta U \sin(\Omega t), \quad \frac{\mathrm{d}\eta}{\mathrm{d}t} = \omega\xi + \Delta U \cos(\Omega t), \tag{22}$$

where we recall that $\omega$, $\Omega$ and $\Delta U$ are all constants. The system (22) admits a multiply periodic solution of the form

$$\xi(t) = \frac{(\Omega+\omega)\Delta U}{\Omega^2 - \omega^2}[\cos(\Omega t) - \cos(\omega t)],$$
$$\eta(t) = \frac{(\Omega+\omega)\Delta U}{\Omega^2 - \omega^2}[\sin(\Omega t) - \sin(\omega t)], \tag{23}$$

where we call $\omega(k)$ the interaction frequency and $\Omega$ the system rotation frequency. The solution (23) shows that a periodically oscillating solution is obtained for small vortex separations $r$, corresponding to a regime in which the vortices oscillate about each other with frequency $\omega(k)$, given by (21), and rotate as a system about some common centre with frequency $\Omega$ (as observed in figure 4). The maximum vortex separation is proportional to $(\Delta U)(\Omega+\omega)/(\Omega^2 - \omega^2)$, so that when either $\Delta U$ is large or $\Omega$ and $\omega$ approach each other (which corresponds to a resonant interaction of the three-vortex system), the separation distance $r$ between the vortices will no longer be small. Such a case is demonstrated by our previous calculations with three circular vortices shown in figure 5, resulting in tearing of the initially aligned vortex pair.

## 5. Results for three deformable vortices

In this section, we use the contour dynamics and discrete vortex methods described in §§3.1 and 3.2 to examine the deformation of the vortex core caused by the induced baroclinic velocity of the vortices, and the effect of core deformation on vortex tearing. Most of the calculations are performed using contour dynamics, but discrete vortex

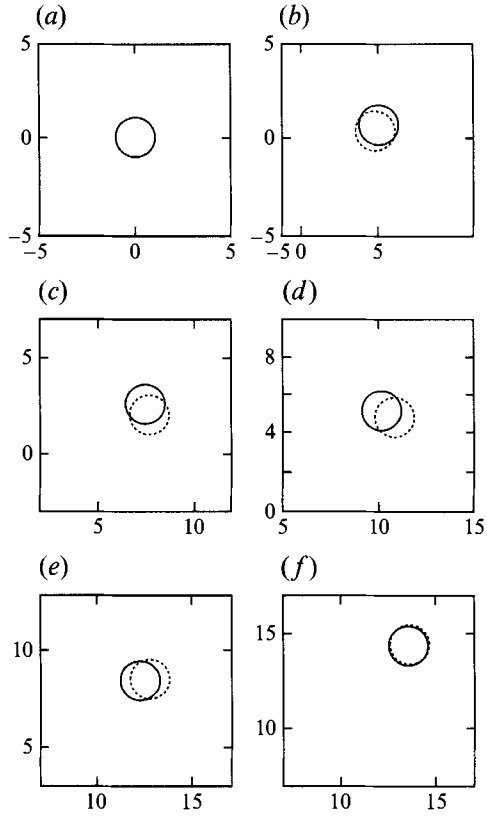


FIGURE 6. Vortex contours for a non-tearing case with the same parameter values as in figure 4, but computed with the contour dynamics method. The upper- and lower-layer vortices are denoted by solid and dashed curves, respectively. The frames are shown at the following times: (*a*) $t = 0$, (*b*) 80, (*c*) 160, (*d*) 240, (*e*) 320, (*f*) 440.

simulations are used in cases where the vortices become very deformed or break up. We also examine the influence of various parameters, such as $k$, $\delta$ and $q_1/q_2$, on the vortex motion in both the tearing and non-tearing regimes. In all cases examined, it is found that the two initially aligned vortices remain close to each other for all time if $\Delta U$ is less than some critical value $\Delta U_{crit}$ and that the vortices exhibit large separation for $\Delta U$ greater than this critical value. However, the degree of vortex deformation during the motion, and subsequently the critical value of $\Delta U$, is somewhat affected by the values of the dimensionless parameters governing the system.

Typical vortex behaviour observed for low values of $k$ ($k < 1$) is shown in figure 6 at six different values of time for the same parameter values as used in plotting the paths of three circular vortices in figure 4. In figure 6, as well as in subsequent calculations done with contour dynamics, the contour of the upper-layer vortex is denoted by a solid curve and that of the lower-layer vortex by a dashed curve. The third vortex, which is not shown, generates a current from left to right (initially) which is stronger in the upper layer than in the lower layer. The circulation of the vortices is counterclockwise in all cases. We see that initially the upper vortex is carried downstream by the current, but that the mutually induced motion of the two vortices causes them to rotate counterclockwise about their mutual centre. As this rotation continues, the upper-layer vortex is carried upstream (against the current) and the

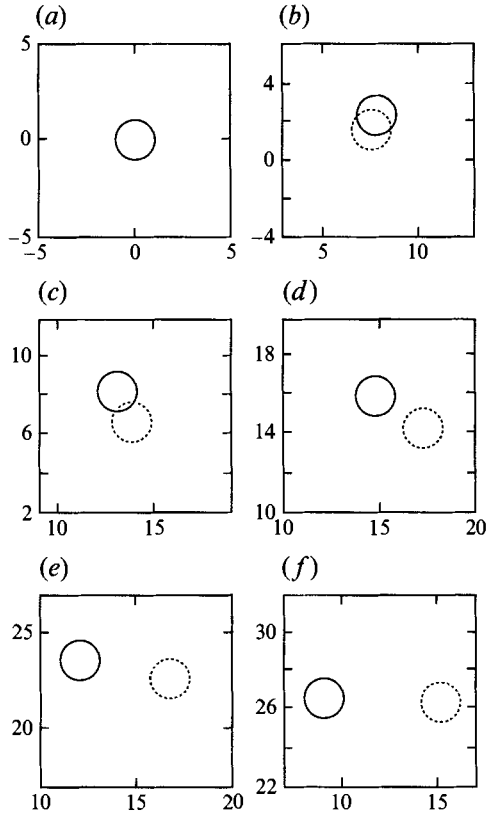


FIGURE 7. Vortex contours for a tearing case with the same parameter values as in figure 5. The frames are shown at the following times: (*a*) $t = 0$, (*b*) 80, (*c*) 160, (*d*) 240, (*e*) 320, (*f*) 360.

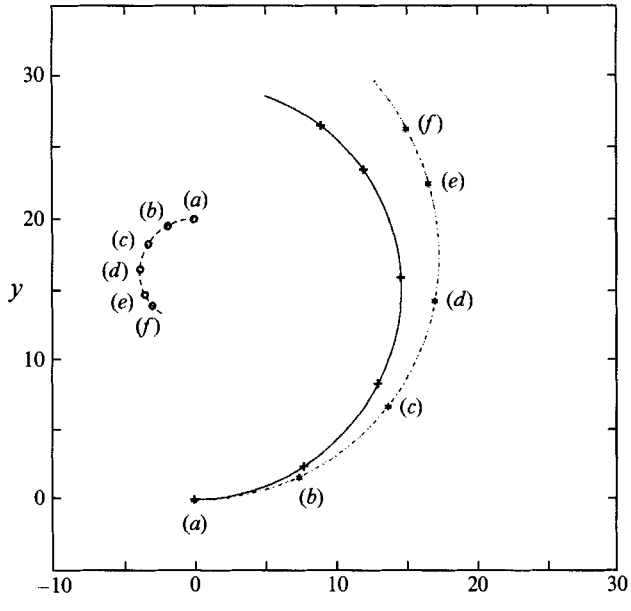


FIGURE 8. Vortex paths for the tearing case shown in figure 7 computed with the contour dynamics method. The vortex locations at the six frames in figure 7 are denoted by symbols marked on the curves next to the corresponding frame letter.

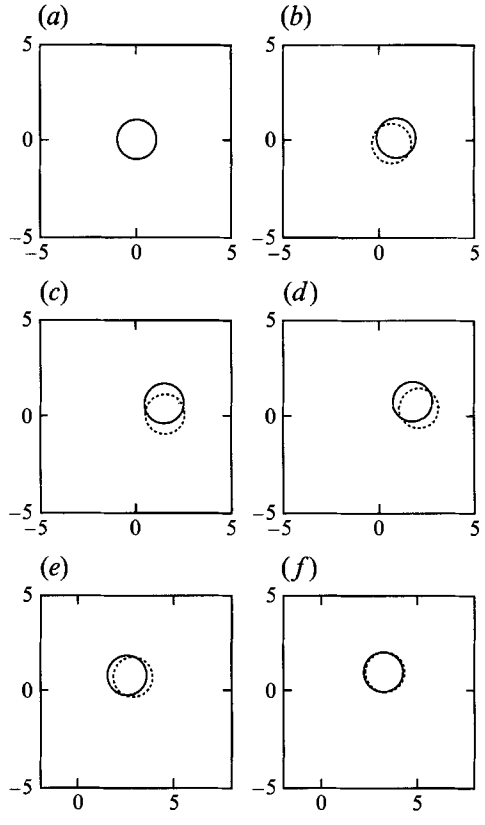


FIGURE 9. Vortex contours for a non-tearing case with $\delta = 0.1$ and other parameters as in figure 4. The frames are shown at the following times: (*a*) $t = 0$, (*b*) 80, (*c*) 160, (*d*) 240, (*e*) 320, (*f*) 380.

lower-layer vortex is carried downstream, until after a while the upper-layer vortex is upstream of the lower-layer vortex. The current then carries the upper-layer vortex back downstream until the two vortices are exactly on top of each other at $t = 440$. The relative motion of the two vortices seems to be periodic in time, although the vortex pair as a whole is transported in the direction of the current (in a rotation about the third vortex) during each period of oscillation. It is also observed that the vortices maintain a nearly circular shape throughout the motion.

A case demonstrating tearing of the vortices is show in figure 7 for the same parameter values as previously used in figure 5 for circular vortices. The paths of the centroids of the vortices are plotted in figure 8, and the vortex locations at the six different times shown in figure 7 are marked by symbols. Because of the rotation of the vortex system about the third vortex, the current acts nearly from right to left in frame (*f*) of figure 7, whereas it initially acts from left to right in frame (*a*). In the case in which vortex tearing occurs, the upper-layer vortex rotates more rapidly about the third vortex than the lower-layer vortex. The vortices are again observed to remain nearly perfectly circular and the results correspond closely to those shown in figure 5 of the previous section.

As the parameter $k$ is increased, the oscillation frequency $\omega(k)$ of the initially aligned vortex pair is predicted from the linear theory of the previous section (equation (21)) to increase. The critical current difference similarly increases as the value of $k$ increases,

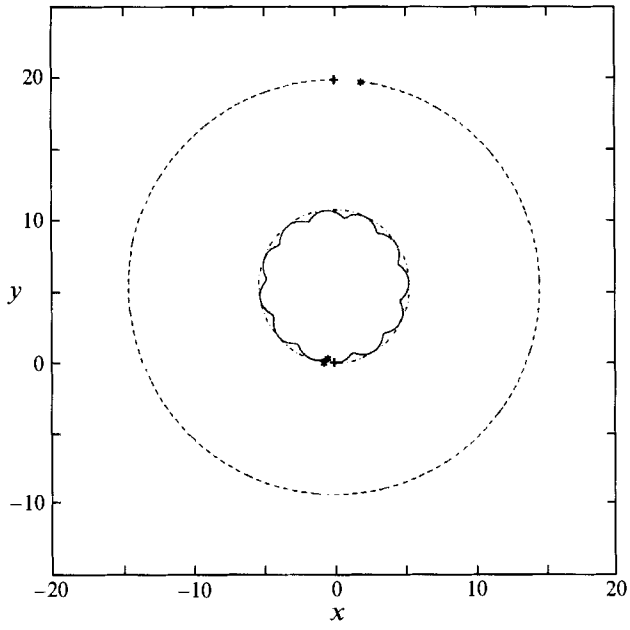


FIGURE 10. Vortex paths for the case shown in figure 9 with $\delta = 0.1$, showing uneven vortex displacement and reduction in $\Omega$ for small values of $\delta$. The curves and symbols have the same meaning as in figure 4, and the computation was stopped at $t = 3600$.

but there is no other qualitative difference in the results from those already shown. We have previously noted that for larger values of $k$ (e.g. $k > 1$) the current difference between the layers becomes extremely small for $d \gg 1$ since $K_1(kd)$ decays exponentially for large $kd$, and so the investigation in the present section is restricted to small $k$-values. It is known that baroclinic vortex pairs with $k > 1$ and appropriate values of separation between the vortex centroids can exhibit an 'alignment' process, similar to a vortex merger in two-dimensional flow, which causes a great deal of deformation of the vortices (Polvani 1991). While we are able to match Polvani's computations with $k > 1$ using our contour dynamics code, the range of $k$-values used in the present vortex tearing calculations is too small for the alignment process to occur.

The effect of relative layer depth on the vortex motion is illustrated in figure 9 for the case of a shallow layer overlying a much deeper layer, with $\delta = 0.1$ and all other parameters the same as in figure 4. The results in figure 9 appear to be very similar to those shown in figure 6 with equal layer depths, although the displacement of the pair as a whole is substantially less for the $\delta = 0.1$ case than for $\delta = 1$ even though the imposed currents in each layer from the third vortex are the same. The paths of the vortex centroids (computed with circular vortices) for $\delta = 0.1$ (shown in figure 10) contrast markedly with that calculated for the $\delta = 1$ case (shown in figure 4), even though all other parameters are the same. In comparing figures 4 and 10, it is noted that the time period required for oscillation of the pair of initially aligned vortices is fairly close in the two cases ($t = 440$ for $\delta = 1$ and $t = 380$ for $\delta = 0.1$) and in both cases somewhat above the value predicted by (21) using the linear theory for $k = 0.2$ ($t = 280$). The strength of all the vortices are also the same in both cases, such that the circulation of the third vortex is about four times greater than that of the two initially aligned vortices. It is therefore strange to observe in figure 10 that the third vortex has moved a much longer distance than the two weaker vortices, whereas in figure 4 the

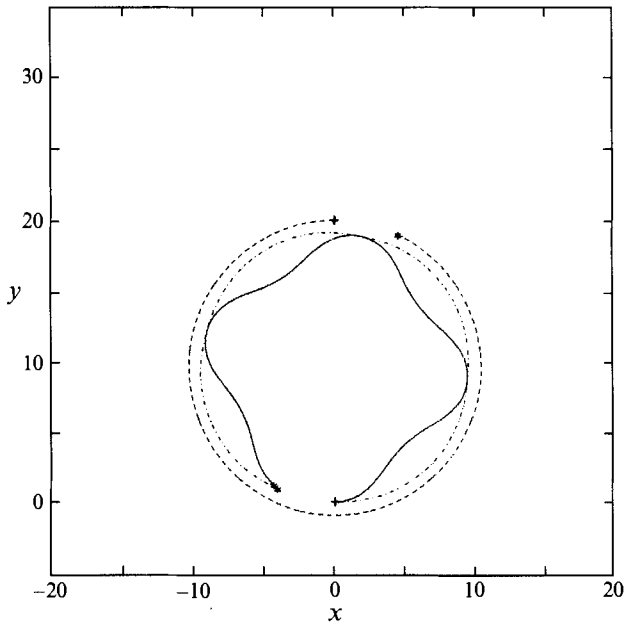


FIGURE 11. Vortex paths with $\Delta U = 0.0125$, which is just below the critical value 0.0138, showing increase of the vortex interaction period as $\Delta U$ approaches the critical value. All other parameters are the same as in figure 10. The computations are stopped at $t = 2400$.

weaker vortices move a longer distance than the stronger third vortex, as would be expected. This difference arises from the fact that the upper-layer vortex must 'drag along' the lower-layer vortex in the non-tearing regime, through their baroclinic interaction, such that the separation distance between the two vortices remains small during their mutual rotation about the third vortex. When $\delta = 0.1$, the lower-layer vortex is much deeper than the upper-layer vortex, which causes the pair as a whole to rotate more slowly about the third vortex than in the case with equal layer depths. The upper-layer vortex also exhibits larger amplitude motion during oscillation of the initially aligned vortex pair than the lower-layer vortex, which results in the 'bumpy' appearance of the solid curve in figure 10.

Vortex paths are shown in figure 11 for a case with the same parameter values as in figure 10, but a value of current difference ($\Delta U = 0.0125$) that is just below the critical value ($\Delta U_{crit} = 0.0138$) for this case. This critical value of $\Delta U$ for the case with $\delta = 0.1$ is somewhat higher than for $\delta = 1$ (see figure 5) since the rotation frequency $\Omega$ about the third vortex is less. It is generally observed that the oscillation period of the initially aligned vortex pair increases substantially above the value predicted by equation (21) of the linear theory as $\Delta U$ approaches the critical value $\Delta U_{crit}$, and the oscillation period approaches the linear theory prediction for $\Delta U$ much less than the critical value. This effect is clearly apparent in figure 11, in which the oscillation period of the pair has increased to about 600 from the linear theory value of 280 for $k = 0.2$.

The effect of a difference in vortex strengths is illustrated in figure 12 using the contour dynamics method for the case in which the upper-layer vortex is much weaker than the lower-layer vortex ($q_1/q_2 = 0.05$) and all other parameters the same as in figure 4. (Note that the scale of the last two frames in figure 12 is different from that of the first four frames.) The same case is shown using the discrete vortex method in figure 13, but for longer times. Comparison of frames (*b*) and (*c*) of figures 12 and 13

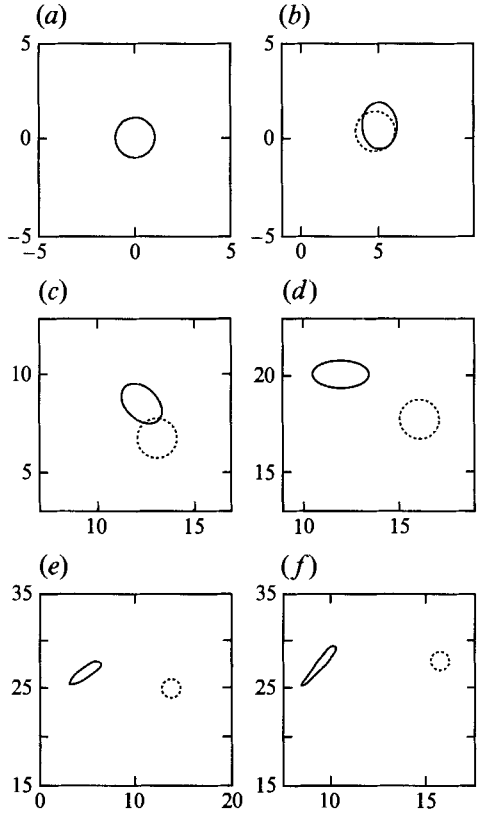


FIGURE 12. Vortex contours for a tearing case showing deformation of the surface vortex for the case $q_1/q_2 = 0.05$. All other parameters are as in figure 4. The frames are shown at the following times: (*a*) $t = 0$, (*b*) 42, (*c*) 168, (*d*) 294, (*e*) 378, (*f*) 420. *The* $x, y$ scale is reduced for the last two frames.

shows excellent agreement between the predictions of these two methods. It is found that the (stronger) lower-layer vortex appears to remain almost circular, whereas the (weaker) upper-layer vortex becomes extremely deformed during the motion. This deformation is believed to initially occur because of the strain imposed on the weaker vortex either by the baroclinic velocity induced by the stronger vortex in the lower layer or by the much stronger, but farther away, third vortex. In the last three frames of figure 13, the weak upper-layer vortex is observed to deform into a vortex sheet and to wrap about the strong third vortex. It is shown by Moore & Saffman (1971), for the two-dimensional case with no Coriolis force, that a vortex in a straining flow becomes deformed by the external straining, and if the strain rate is above a critical value the vortex core will become unstable and elongate indefinitely. It is a simple matter to show that the $1/r$ velocity dependence external to a vortex core in the usual two-dimensional flow exerts a potential straining flow on other vortices in the flow field, and this fact was used by Moore & Saffman (1975) to model vortex pairing in a turbulent mixing layer. It is reasonable to expect a similar type of core instability to occur between two vortices in different layers in a geostrophic flow, since both the baroclinic and barotropic induced velocities of the vortices approach a $1/r$ dependence as the vortices move far apart from each other.

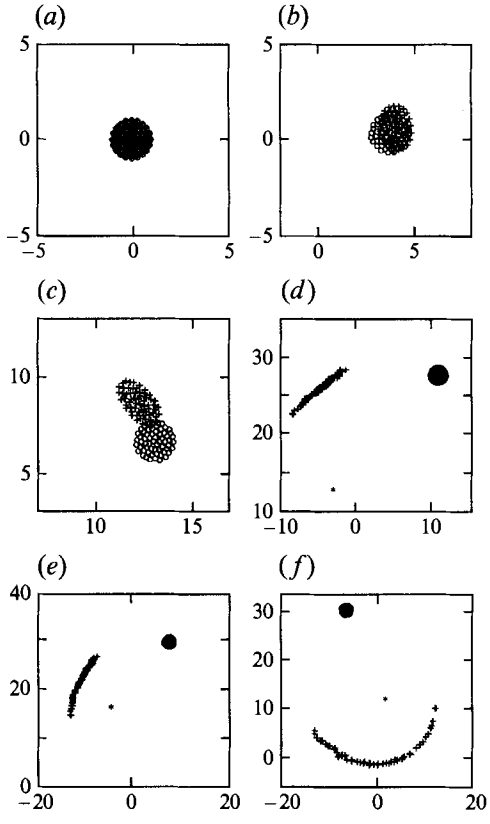


FIGURE 13. Discrete vortex simulation of the case shown in figure 12 with $q_1/q_2 = 0.05$, but for longer times. The frames are shown at the times: (*a*) $t = 0$, (*b*) 42, (*c*) 168, (*d*) 420, (*e*) 462, (*f*) 840.

## 6. Results with non-uniform background potential vorticity

Tearing of a two-vortex system due to interaction with a third vortex was studied in the previous two sections. In the current section, we consider vortex tearing due to some ambient current difference between the layers which is maintained by a background non-uniform potential vorticity field, as given in (8). A secondary flow about the vortices is therefore generated by the rearrangement of the background potential vorticity field by the vortices.

In order to understand the nature of this secondary flow, we first consider the flow caused by a single vortex (but no current) in the upper layer and a current in the negative $x$-direction (but no vortex) in the lower layer. Runs were made using the algorithm described in §3 for cases with the parameters $k = \delta = q_1/q_2 = 1$ and current differences of $\Delta U = -0.1$ and $\Delta U = -1$. Contour plots for the secondary vorticity field $q_{s1}$ in the upper layer are shown in figure 14(*a*) at $t = 2$ and in figure 14(*b*) at $t = 14$. The contours appear as a dipole which is distorted slightly in the direction of vortex rotation. The secondary potential vorticity contours for $\Delta U = -1$ and those for the lower layer with $\Delta U = -0.1$ appear qualitatively similar to those in figure 14(*a*, *b*). After an initial transient period, the contours of $q_s$ seem to achieve a nearly steady state. This trend toward a steady asymptotic state can be observed both from the contour shapes and from plotting the maximum values of $q_{s1}$ with time, as shown in figure 15 for both $\Delta U = -0.1$ and $\Delta U = -1$. The maximum values of $q_s$ in the asymptotic state seem to be of the same order of magnitude as $\Delta U$ and to vary nearly

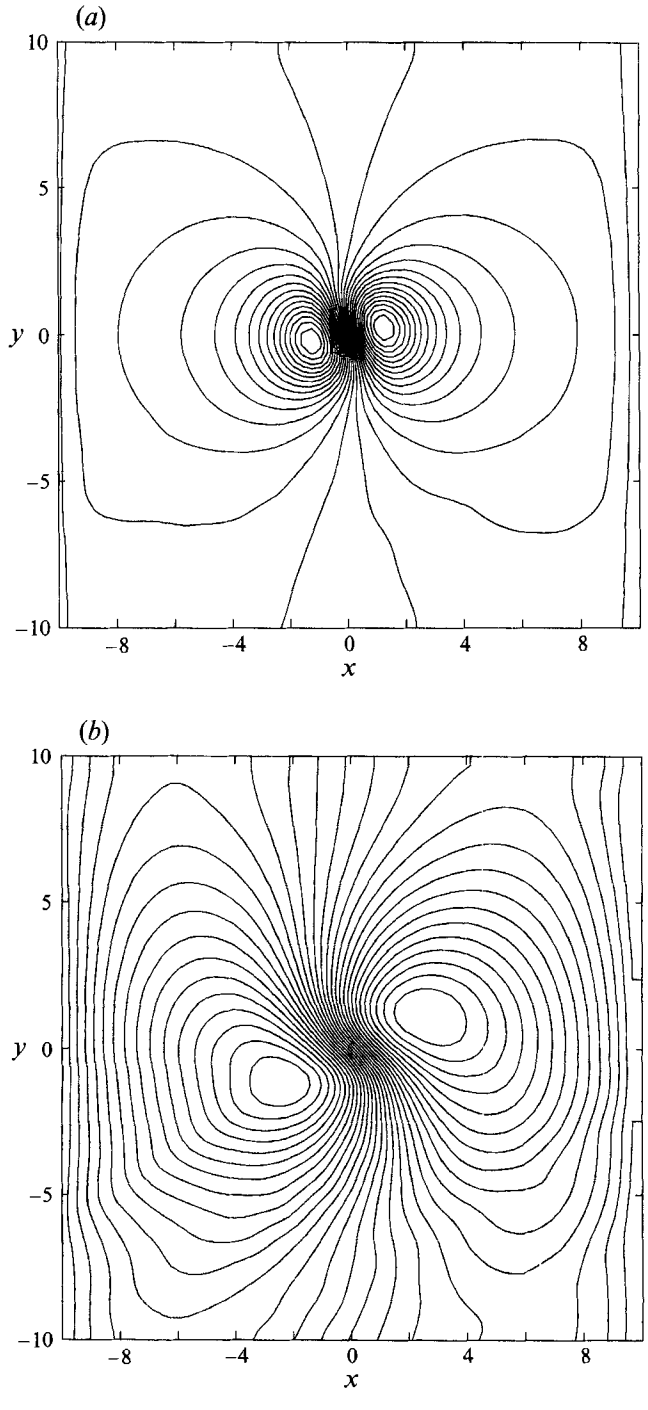


FIGURE 14. Secondary potential vorticity contours in the upper layer for the case of a single vortex (but no current) in the upper layer and current (but no vortex) in the lower layer. The plots are for $k = \delta = q_1/q_2 = 1$ and $\Delta U = -0.1$, and the times in (*a*) and (*b*) are $t = 2$ and 14, respectively.

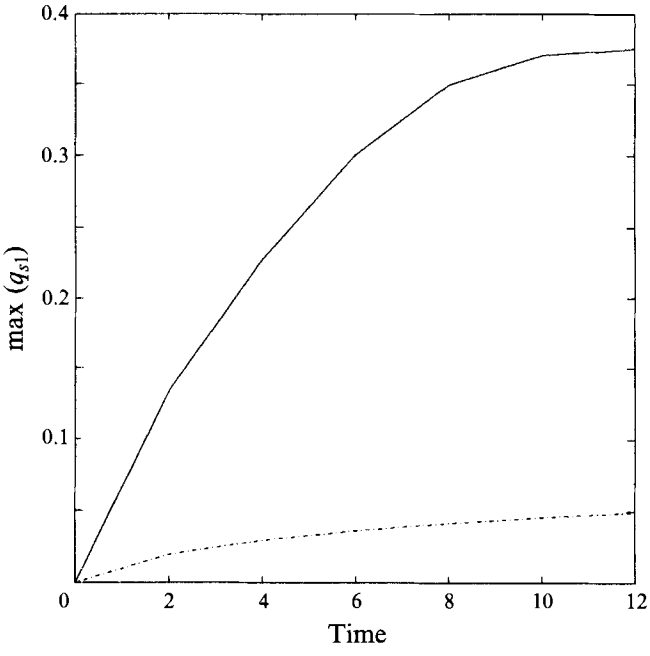


FIGURE 15. Maximum values of the secondary potential vorticity $q_{s1}$ in the upper layer in the single vortex case as a function of time for $\Delta U = -0.1$ (dashed-dotted curve) and $\Delta U = -1$ (solid curve), with $k = \delta = q_1/q_2 = 1$.

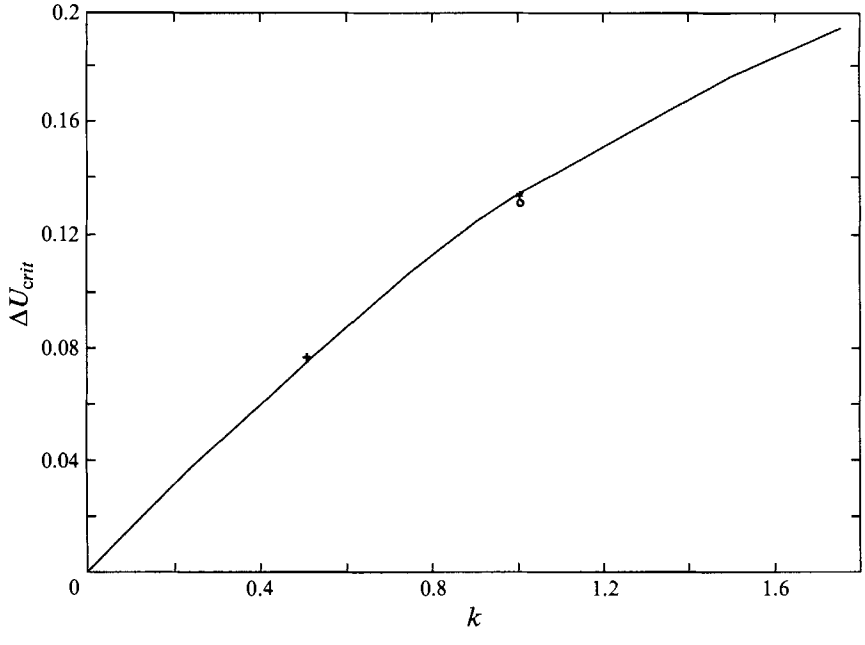


FIGURE 16. Predicted values of the critical $\Delta U$ for the case in which the secondary flow is neglected. Solid curve is obtained from the model equation (24) and the data points are from contour dynamics calculations with $q_1/q_2 = 1$ and the following values of layer depth ratio: +, $\delta = 1$; ○, $\delta = 1$; *, $\delta = 0.1$.

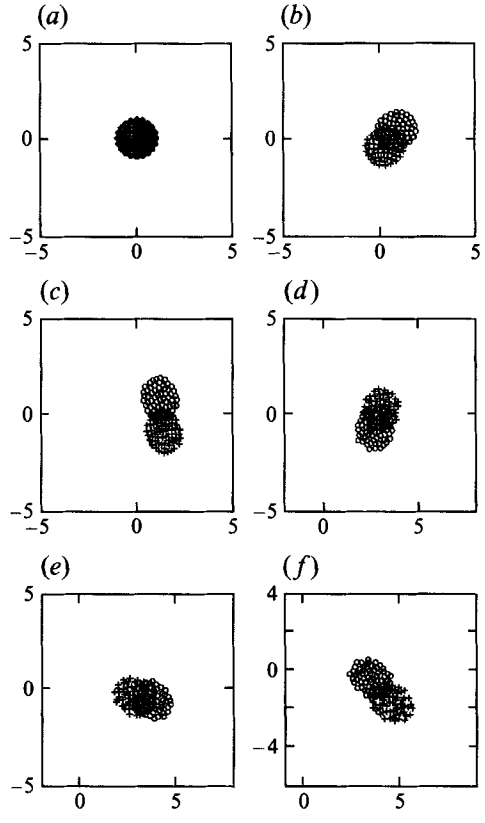


FIGURE 17. Example of a case with no vortex tearing, which includes the secondary flow, for the parameter values $k = \delta = q_1/q_2 = 1$ and $\Delta U = 0.1$. Frames are shown at the following times: (*a*) $t =$ 0, (*b*) 12, (*c*) 24, (*d*) 60, (*e*) 84, (*f*) 132.

proportionally with $\Delta U$, as would be expected from (9). We also mention that the vortex core remains nearly circular for $\Delta U = -0.1$ but deforms somewhat in the direction opposite to that of the current for $\Delta U = -1$. The vortices do not appear to move significantly during the calculations, which typically covered about five rotation periods of the vortex. These results thus differ from those for a vortex in a beta-plane, for which case drifting of the vortex is observed (Reznik 1992).

We note that for sufficiently small $\Delta U$ ($\Delta U \ll 1$) and for $O(1)$ values of $q_1/q_2$, the secondary potential vorticity $q_{sn}$ is very small compared to the potential vorticity $q_1$ or $q_2$ of the vortices. Motivated by this observation, we consider a simple model (similar to that given in §4) in which the vortices are assumed to be circular and the secondary flow associated with $q_s$ is neglected. The governing equations of this model for a separation $\xi$ in the $x$-direction and $\eta$ in the $y$-direction of the upper- and lower-layer vortices are

$$\frac{\mathrm{d}\xi}{\mathrm{d}t} = -\eta f(r) + \Delta U, \quad \frac{\mathrm{d}\eta}{\mathrm{d}t} = \xi f(r), \tag{24}$$

where $f(r)$ is defined by (20). It is noted that only two parameters, $\Delta U$ and $k$, affect the vortex separations in (24). In the small-displacement limit, this system reduces to

$$\frac{\mathrm{d}\xi}{\mathrm{d}t} = -\omega\eta + \Delta U, \quad \frac{\mathrm{d}\eta}{\mathrm{d}t} = \omega\xi, \tag{25}$$

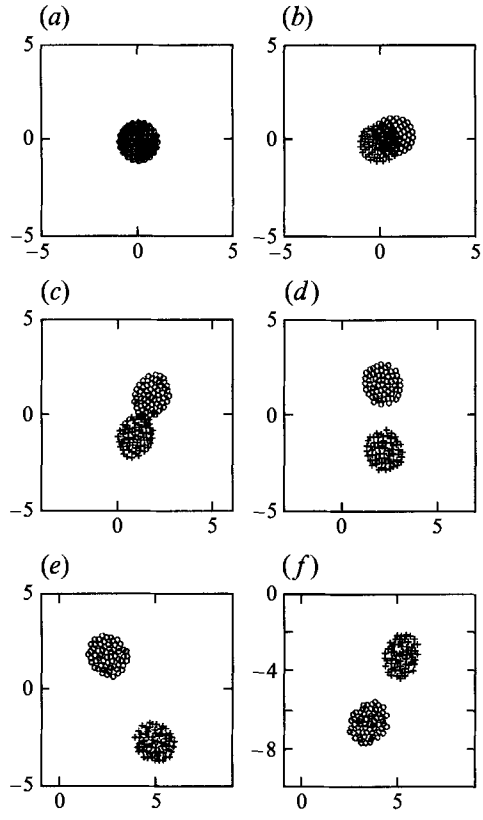


FIGURE 18. Example of a case, with secondary flow, where $\Delta U$ is just above the critical value for tearing from figure 16. The parameter values are as in figure 17, but $\Delta U = 0.15$. Frames are shown at the following times: (*a*) $t = 0$, (*b*) 6, (*c*) 18, (*d*) 30, (*e*) 54, (*f*) 90.

where $\omega(k)$ is given by (21). Equation (25) admits a periodic solution of the form

$$\xi(t) = (\Delta U/\omega)\sin(\omega t), \quad \eta(t) = -(\Delta U/\omega)\cos(\omega t) + (\Delta U/\omega), \tag{26}$$

such that the maximum separation of the vortex centroids is $r_{max} = 2(\Delta U)/\omega$. The nonlinear system (24) was integrated using a fourth-order Runga–Kutta method for various values of $k$ (in the range $0 < k < 2$) to find the critical value of $\Delta U$ for vortex tearing. The results of these computations for $\Delta U_{crit}$ are shown by the solid curve in figure 16, as well as a few numerical data points obtained from the contour dynamics method (neglecting the secondary flow) for deformable vortices. The computations are restricted to $k < 2$, at which point the predicted $\Delta U_{crit}$ has increased to 0.2, since the neglect of the secondary flow is not valid for large $\Delta U$.

Computations of vortex tearing which include the effect of the secondary flow were also performed, using the alternative algorithm based on Green's functions described in §3.3, and the results were compared to those without the secondary flow. For cases with $\Delta U$ well below the predicted critical value in figure 16, the vortices are observed to oscillate about each other (as shown in figure 17 for $k = \delta = q_1/q_2 = 1$ and $\Delta U = 0.1$), but not to return to the initial state in which one vortex lies on top of the other at the end of the period, as was observed to be the case without secondary flow (recall figure 6). For $\Delta U$ slightly above the predicted critical value in figure 16, the vortices still seem to rotate about each other, but the separation distance between the vortices

increases dramatically (as shown in figure 18, for the same parameter values as in figure 17 but with $\Delta U = 0.15$). There does not appear to be a clear bifurcation between the tearing and non-tearing states, as was the case without secondary flow, but instead the vortices oscillate with a separation distance that appears to increase with time. The calculations were stopped when the vortices got too close to the edge of the grid, so the long-time behaviour of the system is not known. For yet higher values of $\Delta U$, considerably above the critical values given in figure 16, the vortices tore apart with only slight deflection from the baroclinic induction.

## 7. Conclusions

This study uses the two-layer quasi-geostrophic equations to determine conditions under which a vortex can extend through two layers, in which there exists a current difference between the layers, without large separation of the parts of the vortex in the different layers. The ability to withstand current variations along the vortex core, sometimes of an order of magnitude or more, is a commonly observed feature of strong geophysical vortices such as cyclones and ocean rings.

We have found that the dynamics of the vortex tearing process depends on the way in which the current difference is maintained. For cases in which the current difference is generated by a third vortex, both analytical and numerical results have been obtained which show that if the current difference $\Delta U$ between the layers is below a critical value, the two initially aligned vortices will oscillate periodically about each other with only a small separation of their centroids. The vortex separation decreases as the current difference $\Delta U$ decreases, such that if $\Delta U$ is small enough a vortex might appear to simply extend through the two layers with little observable effect of the current difference. For values of $\Delta U$ above the critical value, a bifurcation occurs in which the separation distance between the vortices becomes large and the vortices are said to be torn by the current.

The effects of unequal layer depths and unequal vortex strengths are studied by variation of the parameters $\delta$ and $q_1/q_2$. It is found that the relative layer depth affects the rotation rate $\Omega$ of the initially aligned vortices about the third vortex, which subsequently influences the critical current difference $\Delta U_{crit}$ for tearing to occur. A difference in strength between the upper- and lower-layer vortices, on the other hand, can have a strong effect on the vortex deformation, causing the weaker vortex to become greatly deformed due to the baroclinic induced flow from the stronger vortex. For most cases examined with vortices of nearly equal strength, however, the vortices remain nearly circular during their motion and a simple analysis based on perfectly circular vortices convected at their centroids yields results in good agreement with the more exact contour dynamics calculations.

Examples are also considered in which the current difference is generated by a non-uniform ambient potential vorticity in the two layers. In this case, a secondary flow occurs due to the redistribution of the background potential vorticity by the vortex flow. This secondary flow is found to have only a slight effect on the vortex tearing process for small values of $\Delta U$.

A more detailed study of the effect of non-uniform background potential vorticity than we have offered here is probably necessary in applying this work to many oceanic or atmospheric flows. In particular, the secondary flow caused by the beta-effect may have a significant influence on the critical current difference for tearing for vortices of large horizontal dimension. Also, in many geophysical problems the current difference to which vortices are subject is generated by shearing, such as for wind-driven currents

in the oceanic surface layer or for atmospheric flows within the planetary boundary layer. If the shearing causes a substantial change in potential vorticity during a period of oscillation of the aligned vortex pair, the analysis in the paper may not apply. A final shortcoming of the paper is that many vortices that resist tearing in the oceans and atmosphere are quite strong and are not well described by quasi-geostrophic dynamics. It may therefore be necessary to incorporate ageostrophic effects to accurately describe tearing of such vortices.

While there is obviously a great deal of work that can be pursued in this topic, the basic vortex interaction which gives rise to the ability of a vortex in a stratified quasi-geostrophic flow to withstand a current difference along its axis is clearly brought out in the present paper, and we expect that this mechanism will not be qualitatively changed by further complication of the flow. Moreover, the specific predictions of the present paper seem to be reasonable for geophysical flows. For example, in a two-layer model of a tropical oceanic flow, typical values of $k$ and $\delta$ are about 0.8 and 0.05, respectively. If we take the values of $q$ for the upper- and lower-layer vortices as equal, the critical value of the dimensionless current difference between the layers (for the case where the current is maintained by a non-uniform background potential vorticity field) is about 0.12. Recalling that current is non-dimensionalized by the product $Rq$ in this case, where $R$ is the vortex core radius, it is found that tearing of the vortex pair occurs when $Rq$ is less than about eight times the ambient current difference between the layers, and no tearing occurs if $Rq$ is greater than this value. The analysis thus confirms what one might intuitively expect, that stronger and wider vortices are more able to resist tearing by a current difference than weaker, thin vortices. Since the maximum velocity magnitude $u_{max}$ in a vortex is about $\frac{1}{2}Rq$ (for a Rankine vortex) and taking a typical value of ambient current difference $\Delta U$ of about 0.1 m/s for oceanic flows, we find that an oceanic vortex will be able to resist tearing if $u_{max}$ is above about 0.4 m/s, which might be expected in strong ocean rings.

## REFERENCES


AREF, H. & POMPHREY, N. 1982 Integrable and chaotic motions of four vortices. I. The case of identical vortices. *Proc. R. Soc. Lond.* A **380**, 359–387.

EIDE, L. I. 1979 Evidence of a topographically trapped vortex on the Norwegian continental shelf. *Deep-Sea Res.* **26**, 601–621.

FLIERL, G. R. 1987 Isolated eddy models in geophysics. *Ann. Rev. Fluid Mech.* **19**, 493–530.

FLIERL, G. R. 1988 On the instability of geostrophic vortices. *J. Fluid Mech.* **197**, 349–388.

GORDON, A. L. 1978 Deep Antarctic convection west of Maud Rise. *J. Phys. Oceanogr.* **8**, 600–612.

GRIFFITHS, R. W. & HOPFINGER, E. J. 1986 Experiments with baroclinic vortex pairs in a rotating fluid. *J. Fluid Mech.* **173**, 501–518.

GRIFFITHS, R. W. & HOPFINGER, E. J. 1987 Coalescing of geostrophic vortices. *J. Fluid Mech.* **178**, 73–97.

GRYANIK, V. M. 1983 Dynamics of singular geostrophic vortices in a two-layer model of the atmosphere (or ocean). *Izv. Atmos. Ocean. Phys.* **19**, 171–179.

HELFRICH, K. R. & SEND, U. 1988 Finite-amplitude evolution of two-layer geostrophic vortices. *J. Fluid Mech.* **197**, 331–348.

HOGG, N. G. 1973 The preconditioning phase of MEDOC 1969 – II. Topographic effects. *Deep-Sea Res.* **20**, 449–459.

HOGG, N. G. & STOMMEL, H. M. 1985 The heton, an elementary interaction between discrete baroclinic vortices, and its implications concerning eddy heat-flow. *Proc. R. Soc. Lond.* A **397**, 1–20.

KILLWORTH, P. D. 1979 On 'chimney' formations in the ocean. *J. Phys. Oceanogr.* **9**, 531–554.

MOORE, D. W. & SAFFMAN, P. G. 1971 Structure of a line vortex in an imposed strain. In *Aircraft Wake Turbulence* (ed. J. H. Olsen, A. Goldburg & M. Rogers), pp. 339–353. Plenum.

MOORE, D. W. & SAFFMAN, P. G. 1975 The density of organized vortices in a turbulent mixing layer. *J. Fluid Mech.* **69**, 465–473.

ORSZAG, S. A. & GOTTLIEB, D. 1980 In *Approximation Methods for Navier–Stokes Problems.* Lecture Notes in Mathematics, Vol. 771, pp. 381–398. Springer.

PEDLOSKY, J. 1979 *Geophysical Fluid Dynamics.* Springer.

POLVANI, L. M. 1991 Two-layer geostrophic vortex dynamics. Part 2. Alignment and two-layer V-states. *J. Fluid Mech.* **225**, 241–270.

POLVANI, L. M., ZABUSKY, N. J. & FLIERL, G. R. 1989 Two-layer geostrophic vortex dynamics. Part 1. Upper-layer V-states and merger. *J. Fluid Mech.* **205**, 215–242.

PULLIN, D. I. 1992 Contour dynamics methods. *Ann. Rev. Fluid Mech.* **24**, 89–115.

REZNIK, G. M. 1992 Dynamics of singular vortices on a beta-plane. *J. Fluid Mech.* **240**, 405–432.